Intrinsic optical nonlinearity in colloidal seeded grown CdSe/CdS nanostructures: Photoinduced screening of the internal electric field

Giovanni Morello,* Fabio Della Sala, Luigi Carbone, Liberato Manna, Giuseppe Maruccio, Roberto Cingolani, and Milena De Giorgi

National Nanotechnology Laboratory (NNL) of CNR-INFM, Distretto Tecnologico ISUFI, Università del Salento, Via per Arnesano, 73100 Lecce, Italy

(Received 10 January 2008; revised manuscript received 15 October 2008; published 13 November 2008)

The assessment of the presence and the origin of an intrinsic internal electric field in novel colloidal CdSe/CdS nanoheterostructures is of fundamental importance in order to understand their optical properties, due to both their impact on the basic research fields, and their potential in technological applications. To this aim, a deep study of the carrier dynamics in spherical (quantum dots) and rod-shaped (nanorods) colloidal seeded grown CdSe/CdS nanocrystals via time-resolved photoluminescence spectroscopy has been carried out in this report. A transient, power-dependent redshift of the spectra is observed. An optical nonlinearity is also found by continuous-wave photoluminescence measurements on ensemble and single nanostructures, which is attributed to a photoinduced screening of an internal field. This internal field could originate from the intrinsic piezoelectric polarization, which is a typical effect in strained heterostructures with a lattice mismatch greater than 3.9%. Our theoretical calculations support the experimental results.

DOI: 10.1103/PhysRevB.78.195313 PACS number(s): 73.21.La, 78.67.Hc, 77.65.Ly, 78.47.Cd

I. INTRODUCTION

In the last few years, novel colloidal synthesis techniques have allowed nanocrystals (NCs) of different sizes and shapes to grow.[1,2] Due to their peculiar optical properties, colloidal NCs show increasing potential as active components in several types of devices, such as lasers,[3] photovoltaic cells,[4] and light emitting diodes.[5] Besides spherical-shaped quantum dots (QDs), other materials with more exotic shapes and compositions have been fabricated and studied optically.[2,6,7] One of the most intriguing nanostructures is based on the growth of a CdS rodlike shell onto a spherical CdSe QD.[8–10] Previous studies[11,12] show that in such a system carriers might experience different types of localization, since the hole remains confined inside the CdSe dot, whereas the electron is completely delocalized throughout the CdS nanorod. However, more recent optical studies on such core/shell dot/rod NCs (Ref. 9) have showed high photoluminescence quantum yield (PLQY) and radiative recombination occurring in the core despite carriers being generated mainly in the shell. This idea that both the electron and the hole are confined in the CdSe core has been very recently confirmed by scanning tunneling spectroscopy measurements.[13] Single rod experiments have revealed a Stark shift induced by a fluctuating charge on the CdS surface,[14] whereas time-resolved (TR) measurements have demonstrated the viability for exciton storage in such heterostructures.[15]

To exploit the full potential of these new nanomaterials, a deeper knowledge of their properties is however required. Among the peculiarities of such nanostructures there is, for instance, the possible existence of an internal field that may affect their electrical and optical properties by means of a Stark shift of the excitonic transitions. Several experiments have studied the permanent dipole moment in colloidal QDs and nanorods (NRs) with both wurtzite and zinc-blende structures.[16–20] The well established existence of the permanent ground-state dipole moment along the *c*-crystallographic axis in CdSe wurtzite NRs (Ref. 17) and QDs (Ref. 19) relies on the crystallographic deviation from the ideal wurtzite structure and it has been found to scale with the nanostructure volume.[17] On the other hand, a permanent dipole moment in zinc-blende nanostructures is attributed to the existence of a surface charge distribution.[18] The surface charge density found by Krishnan *et al.*[20] should not be present in our rods because the rod long axis is aligned with the *c*-crystallographic axis.[8–10]

When heterostructures are considered, a further contribution should be taken into account, which generates an internal field, namely, the piezoelectric polarization induced by both the high piezoelectric constants and the elastic strain due to the lattice mismatch (greater than 3.9%) between the materials constituting the heterostructures.[21–23] Many studies of the internal piezoelectric field have been carried out on GaN-based nanomaterials, typically QDs (Refs. 24 and 25) and quantum wells (QWs),[26–30] on self-assembled InAs QDs,[31] CdSe/CdS systems,[22] and ZnO-based QWs.[32] Continuous-wave (CW) and time-resolved photoluminescence (TRPL) studies of nanostructures having an internal electric field generally show a blueshift of the spectra upon increasing carrier generation rates. In particular, time-resolved measurements have shown a dynamical redshift of the photoluminescence (PL) spectrum in the multiexciton generation regime due to a photoinduced descreening of the internal electric field. So far, however, there has been no evidence of such charge-carrier screening in colloidal nanostructures.

In this paper we show the existence of an internal field in nanosized colloidal CdSe/CdS heterostructures (both spherical and asymmetric dot/rod core/shell structures) by performing TRPL measurements at the picosecond time scale and continuous-wave PL, both on ensemble and single nanostructures, as a function of the excitation power. The experimental results have been interpreted using results from

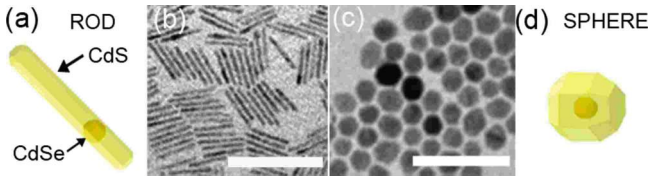

FIG. 1. (Color online) (a) Sketch of an asymmetric CdSe/CdS dot/rod. (b) Low magnification TEM image of CdSe/CdS NRs. (c) Low magnification TEM image of spherical CdSe/CdS nanocrystals with a thick CdS shell. (d) Sketch of a spherical CdSe/CdS nanocrystal. Scale bars are 100 nm long.

effective-mass calculations. We analyzed the contributions of the spontaneous and piezoelectric polarization and attribute the observed nonlinear effect to the piezoelectric polarization induced at the core/shell interface.

II. MATERIALS AND EXPERIMENTAL SETUP

CdSe/CdS NRs [Fig. 1(b)] (core diameter of 4 nm, rod length of 50 nm) and QDs [Fig. 1(c)] (with the same core diameter and total diameter of about 20 nm) were prepared following the method described by Carbone *et al.*[9] The effective dimensions of nanoparticles were estimated by transmission electron microscopy (TEM) analysis.

Single NR spectra were recorded at room temperature by means of a confocal microscopy system (FV-1000 Olympus) in epilayer configuration. The NRs were deposited by drop casting a highly diluted toluene solution (in a nanomolar concentration range) on a cover glass slide. On the slide, the average inter-dot/rod distance was in the order of several microns [see Fig. 2(a)] which allowed for reproducible measurements at single nanoparticle level with submicrometer resolution (about 200 nm). The PL emission was dispersed by a monochromator (0.32 m focal length) and detected by a Si-charge coupled device (CCD) camera. The rods were excited by a diode laser (405 nm) passed through an objective lens ×60, oil immersion, with numerical aperture (NA) =1.4. The laser power was varied from 1% to 20% of the maximum available power (1 mW), corresponding to an excitation power of 10 and 200 μW, respectively. We estimate the average number of electron-hole pairs excited per rod as $N=\phi_p\sigma_{ab}$, where ϕ_p is the photon fluence and σ_{ab} is the absorption cross section of the rod. σ_{ab} is expressed as $\sigma_{ab}=V\alpha_0|f|^2$, where V is the volume of the rod, α_0 represents the absorption coefficient of the CdS bulk (at 3 eV), and $|f|^2$ is a coefficient accounting for local-field effects.[33] By fixing $\alpha_0=8.5\times10^4$ cm^{-1} to the CdS bulk value[34] and $|f|^2=0.55$ (see Ref. 33 for details on calculations and Ref. 35 for the parameter values) we found $\sigma_{ab}=12\times10^{-14}$ cm^{-2}. Considering that the rod PL typically decays in 11 ns, a laser spot diameter of 200 nm and an excitation power of 10 μW give a number of about 0.9 electron-hole pairs per excitation, corresponding to a single exciton generation regime, whereas for higher excitation powers (up to 200 μW) multiexciton generation is expected.

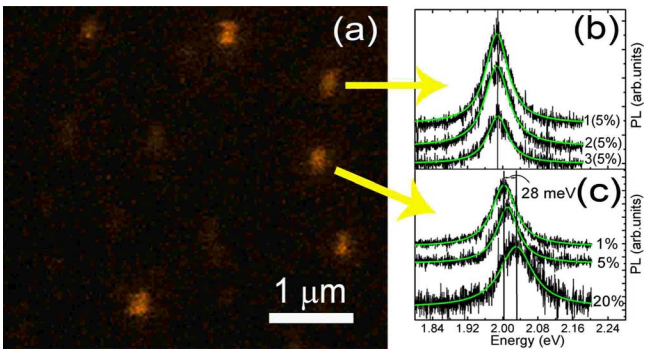

FIG. 2. (Color online) (a) Image of a random field of single NRs acquired by scanning the sample across a diffraction-limited laser spot of a confocal microscope. The sample is prepared by drop casting a nanomolar NR solution onto a cover glass and by rapidly blowing off the solution by means of a strong nitrogen flow. (b) Spectra collected consecutively from a single rod (black lines) [identified by the arrow in panel (a)] obtained at the same laser power and relative Lorentzian best fit curves (green lines). (c) PL spectra from a single rod (black lines) [indicated by arrow in panel (a)] obtained by varying the excitation power, from 1% to 20% of the maximum available power (1 mW), and relative Lorentzian best fit curves (green lines). A clear blueshift is observed when the power is increased.

Ensemble TRPL measurements were performed at room temperature. The samples were excited by the 80 fs pulse of the second harmonic (397 nm) of a Ti:sapphire laser (repetition rate of 80 MHz). The PL signal was dispersed by a spectrograph (0.35 m focal length) and detected by a streak camera (temporal resolution of about 12 ps). The measurements were performed by varying the excitation density from 0.05 to 107 μJ/cm^2 per pulse. Here, N is referred to the average number of electron-hole pairs generated per laser pulse. Considering a laser spot diameter of 40 μm and the same value used in CW excitation for σ_{ab}, we found that for excitation densities until 4 μJ/cm^2 a single exciton regime holds ($N\leq1$), whereas for higher excitation densities multiexciton generation is obtained. In order to avoid spectral effects due to NC orientation, and/or energy transfer among the rods, the NCs were studied in low-density solution (micromolar concentration).

III. EXPERIMENTAL RESULTS

The sketches and the TEM images of the samples studied are reported in Fig. 1. PL measurements were carried out on several single nanostructures. Figures 2(b) and 2(c) show the typical PL spectra, recorded at constant [Fig. 2(b)] and variable [Fig. 2(c)] excitation powers, for two representative NRs. The spectra were recorded by consecutive acquisitions of the signal in a time window of 30 s. By keeping fixed the laser power we observed that the emission energy remains almost constant [Fig. 2(b)]. In some nanoparticles a slight shift (a few meV) both to the blue and to the red occurred during the observations, due to the spectral diffusion, which is often observed in colloidal nanoparticles.[36] With increasing excitation density a significant blueshift of the spectra is observed in all samples [a typical power-dependent behavior is shown in Fig. 2(c)]. The reduced emission intensity in the high power spectra is due to the intermittent emission (blink-

ing) (Ref. 37) observed on such nanostructures under continuous-wave excitation. It has been shown extensively that at high excitation density the blinking is more frequent, leading to a reduction in the integrated PL.[37] In addition, the spectral diffusion (which is more likely to occur at high excitation density) induces too a slight broadening of the PL peak,[38] as can be seen in Fig. 2(c). The observed blueshift is not due to photodegradation[39] because no significant blueshift was detected over time when the NRs were observed at fixed excitation power. In spite of the same power range used, the shift was found to be different from rod to rod, ranging from 14 to 32 meV. Single nanoparticle experiments on similar nanocrystals had been carried out by Müller *et al.*[14] who showed a Stark shift of the optical transitions, which was explained in terms of a fluctuating superficial charge that actually caused the Stark effect. This shift was found to be random in time, as the charge could randomly occupy different superficial sites in a long-time period. To discriminate the role of the superficial charges we have performed optical measurements on ensemble samples. In this way, the effect of charge distribution on the NR surface should be averaged on all the NRs in the ensemble.

Fig. 3(a) shows the PL spectra, and the relative best fits to a Gaussian curve, of CdSe/CdS NRs recorded at two different delay times after the pulsed laser excitation and in both cases at low (2 $\mu J/cm^2$) and high (107 $\mu J/cm^2$) excitation densities. $t=0$ ps corresponds to the shortest delay after the exciting laser pulse, whereas 12 ns is the maximum delay attainable in our system before the subsequent laser pulse comes. Interestingly, at high excitation density the spectrum presents a dynamical redshift, while at low excitation density the emission energy remains unchanged. We plotted the peak energy at different delay times and for different excitation densities [Fig. 3(b)]. The emission energy at long delay times (12 ns) is the same at all excitation densities, whereas largest blueshifts occur at zero time delays, with increasing excitation power [see inset of Fig. 3(b)].

The experimental shifts reported in the inset of Fig. 3(b) can be well fitted to the following saturation function:

$$\Delta E(P) = \Delta E_0 + E_{\text{sat}}(1 - e^{-P/P_0}), \tag{1}$$

where $\Delta E(P)$ represents the difference between the emission energy at 0 ps and that at 12 ns and E_{sat} is the saturation energy. We found a value of E_{sat} of about 22 meV.

This nonlinear effect has been observed also in CW excitation measurements performed at room temperature under argon laser (488 nm) excitation in the range 1–100 mW. In these experiments the blueshift was reduced (down to 8 meV) due to the lower excitation density provided by the CW excitation.

To determine the contribution of the different excitation regimes on the PL lifetimes, we have analyzed the time decays of the PL at different excitation densities. Fig. 4(a) shows the time traces, obtained for excitation density from 2 to 107 $\mu J/cm^2$ and taken on the whole spectral range. In the time window of 2 ns the decay trace at 2 $\mu J/cm^2$ (corresponding to a predicted single exciton regime) is exponential [Eq. (2) with $n=1$], with a typical lifetime of about 11 ns,

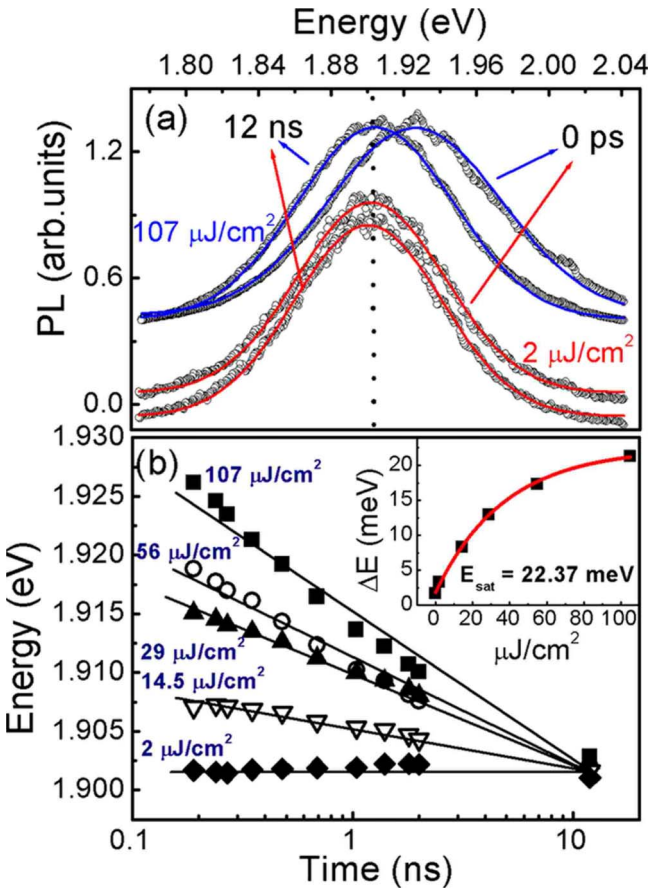

FIG. 3. (Color online) (a) Early and long-time PL spectra (symbols) and relative Gaussian best fits (continuous lines) of CdSe/CdS NRs when excited at high (upper spectra) and low (lower spectra) densities. A blueshift at 0 ps was observed at the maximal power. (b) Transient emission energies measured at different delays after the excitation, recorded at excitation densities ranging from 2 $\mu J/cm^2$, at which no shift was observed, to the maximum value (107 $\mu J/cm^2$) allowed by the experimental setup. Lines are a guide for eyes. Inset: Plot of the shifts as a function of the excitation density (symbols) and best fit of the experimental data to Eq. (1) (continuous line).

whereas by increasing the excitation density (multiexciton regime predicted) the decay curve can be well fitted to a biexponential function [Eq. (2) with $n=2$]

$$I(t) = \sum_{i=1}^{n} A_i e^{-(t-t_0)/t_i}. \tag{2}$$

Here, A_i is the weight for each process and t_i is the relative time constant.

The short time constant (t_1) exhibits a power dependence [Fig. 4(b)]: it ranges from 400 ps (at 107 $\mu J/cm^2$) up to 620 ps (at 14.5 $\mu J/cm^2$). On the contrary, t_2 does not show any dependence on the excitation density, holding an almost constant value of about 11–12 ns comparable to the lifetime of the exponential decay [denoted as t in Fig. 4(c)]. At high excitation power the two decay processes have comparable weights [see inset of Fig. 4(b)], while the fastest process becomes less and less important at low excitation density.

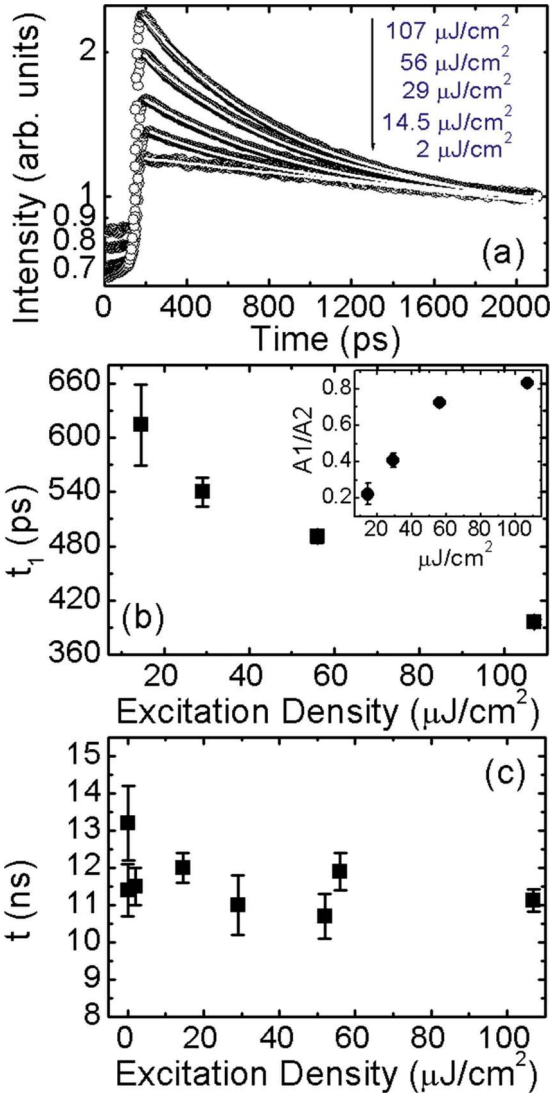

FIG. 4. (Color online) (a) Power-dependent PL decays (logarithmic) normalized to the long-term decay values (symbols) and best fit to Eq. (2) (continuous lines). (b) Power dependence of the shortest lifetime. Inset: Plot of the relative weight ratio A1/A2 of the respective t_1 and t_2 lifetimes vs excitation density. (c) Power dependence of the longest lifetime. The almost constant value at the different excitation densities indicates that such lifetime is related to the single exciton radiative recombination.

The power dependence of both the lifetime and the weight of the fast component is consistent with a typical Auger-type recombination process.[40,41] At maximum excitation power (multiexciton generation) we observe an increase in the Auger recombination rate, as shown by the largest weight and by the smallest time constant of an initial fast PL decay component. By decreasing the excitation power, the fast component vanishes since on average only one exciton should be generated. As in other colloidal QDs,[42] the possible existence of a fine structure[43] of the lowest energy state in such nanostructures could, in principle, explain the nonexponential behavior reported here. The longest decay could in fact be due to emission from dark states and the shortest one to emission from bright states lying at higher energies, which are filled in the high excitation regime. However, the fine structure in such dot/rod core/shell NCs is not known and might deviate from the one of CdSe NCs due to the strain and shape effects.[10,43] Moreover, the typical lifetimes of dark state emission range from microseconds to millisecond,[42,44] far from those observed in our experiments (about 11 ns). Thus, in this context, we can rule out the role of dark states in the emission processes studied and assign the nonexponential decay at high excitation density to Auger recombination.

All these nonlinear optical properties have been observed also on roughly spherical QDs (Fig. 1), which were prepared by growing a thick isotropic CdS shell around the same CdSe cores as those involved in the preparation of the CdSe/CdS NRs.[45] For such spherical QDs we found a maximum blueshift in TRPL experiments of about 18 meV, comparable to the NRs, whereas for what concerns the fastest Auger-type process, the lifetime was on the other hand slightly longer (450–800 ps by decreasing the excitation density) with respect to the rods, probably due to the increased volume in these types of spherical nanocrystals with respect to the NRs.[40]

IV. THEORETICAL RESULTS

In order to understand the electronic structure and the optical properties of these nanocrystals we performed theoretical calculations in the effective-mass approximation.[46] We modeled the dot/rod nanocrystal as a sphere of CdSe material and radius $R=2$ nm inside a hexagonal prism of material CdS and of length $L=50$ nm and radius $R=2.5$ nm. The center of the CdSe sphere is located at a distance $D=L/4$ from the hexagonal basis.[9]

The BenDaniel and Duke variable effective-mass Hamiltonian[47] was solved on a three-dimensional Cartesian grid using the effective-mass parameters from Muller *et al.*[12] (i.e., $m_e=0.13$, $m_h=0.45$ for CdSe; $m_e=0.2$, $m_h=0.70$ for CdS) and energy gaps at room temperature from Landolt-Börnstein[35] (i.e., 1.75 eV for CdSe and 2.5 eV for CdS). Despite CdSe/CdS heterostructures being often reported with a type-II alignment,[22] the conduction-band offset (Δ_c) in CdSe/CdS NRs has been estimated to be zero[12] or very recently to be of type-I ($\Delta_c=0.3$ eV).[13] The latter measurement confirms our photoluminescence excitation (PLE) measurements carried out on such NRs (reported elsewhere[9]) revealing that both electrons and holes are localized in the CdSe core, demonstrating that a type-I system behavior holds in the present case. We consider two different values for the CdSe/CdS conduction-band offset (Δ_c), namely, $\Delta_c=0$ eV (Ref. 12) and $\Delta_c=0.3$ eV.[13] The band offset with the vacuum is fixed to 1.25 eV (see Ref. 48) for both electrons and holes.

In order to model the piezoelectric potential, we consider a simple model for the strain distribution: we assume that the CdSe/CdS nanorod behaves like an epitaxial quantum well, pseudomorphically strained on a CdS substrate. In this way the strain is nonzero only inside the CdSe sphere. This simple model is expected to be more accurate as soon as the diameter of the CdSe sphere approaches the diameter of the

CdS rod, as it is in the samples investigated in this work (note that this model becomes exact if the shape of the CdSe dot is instead cylindrical with the same diameter of the CdS rod). A more detailed investigation, using accurate strain models,[50] will be published elsewhere. The piezoelectric polarization P is then obtained as described in Ref. 26 using piezoelectric coefficients and elastic constants of CdSe and CdS from Landolt-Börnstein.[35] Then we compute the surface polarization charges $\sigma=-\nabla\cdot P$ and we solve a three-dimensional Poisson equation $-\epsilon\nabla^2 V=4\pi\sigma$ (Ref. 49). We consider an uniform dielectric constant $\epsilon=8$. Dielectric mismatch effects[51,52] will be considered elsewhere.

The Poisson equation is solved numerically on the same Cartesian grid used for the electronic structure calculation using the conjugate-gradient technique. The computational grid extends 1 nm in all directions beyond the nanorod: this is enough to ensure that the tails of the wave functions are vanishing small, whereas this is not the case for the electrostatic potential. We computed the electrostatic potential exactly (by inverting the Poisson equation) on the external border of the computational grid, and these computed values are then used as Dirichlet boundary conditions for the Poisson equation. The inversion of the Poisson equation can be done without numerical problem on the external border of the computational grid because here the charge density is zero.

The single exciton energy (E_X) is calculated as $E_X=\Delta E-J_{\mathrm{eh}}$, where ΔE is the energy difference between the first electron and hole quantized state and J_{eh} is the electron-hole Coulomb attraction (i.e., the exciton binding energy). The electron-hole Coulomb attraction is computed as $J_{\mathrm{eh}}=\langle\phi_h|V_e|\phi_h\rangle$, where ϕ_h is the hole wave function and V_e is the electrostatic potential of the electron wave function which is obtained by solving a three-dimensional Poisson equation (as discussed above). The biexciton binding energy is computed as[53–56]

$$B_{XX}=2E_X-E_{XX}=-J_{\mathrm{ee}}-J_{\mathrm{eh}}+2J_{\mathrm{eh}}, \tag{3}$$

where $J_{\mathrm{ee}}=\langle\phi_e|V_e|\phi_e\rangle$ and $J_{\mathrm{hh}}=\langle\phi_h|V_h|\phi_h\rangle$.

In Fig. 5 we report the electron and hole band edges and relative electron and hole wave functions for the rod with and without piezoelectric polarization field. The top panels (a and b) show the band edges and wave functions without any polarization field. In the case of negligible conduction-band offset (panel a) the holes are confined in the CdSe dot, while the electrons are delocalized along the whole structure, as already reported.[8–10] With $\Delta_c=0.3$ eV (panel b) the electron state is also confined in the core[13,57] leading to a much larger exciton binding energy. The calculated values for the transition energies are about 0.1 eV larger than the experimental results. Regarding this point we note that, besides all the approximations of the method, these deviations are related to the uncertainness of the nanocrystal dimensions (in particular the core diameter).

Panel c shows how both the band edges and the wave functions are modified due to the presence of the piezoelectric potential. It is known[58] that the electric field inside a uniformly polarized sphere is uniform and equal to $-P/3\epsilon$,[21,58] where P is the polarization of CdSe and ϵ is the dielectric constant. We obtain a piezoelectric field inside the CdSe sphere of 0.07 V/nm.[23] Panel c shows that both electron and hole wave functions are confined inside the CdSe core due to the piezoelectric field, implying an increased wave function overlap. Note that such behavior is opposite to the usual effect of the piezoelectric field which reduce the electron-hole overlap.[24,26,27]

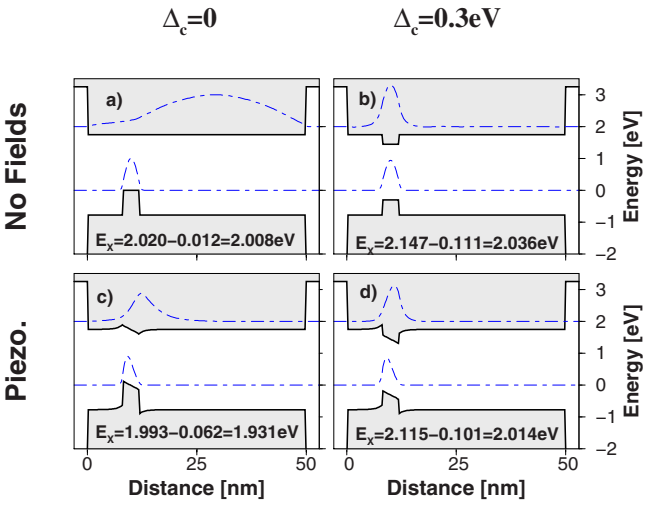

FIG. 5. (Color online) Conduction and valence-band edges and the lowest electron and highest hole wave functions (dot-dashed lines) along the long axis of the rod, obtained from effective-mass calculation. The transition energies $E_x=\Delta E-J_{\mathrm{eh}}$ are also reported (see text for details). Panel (a): no fields and $\Delta_c=0$ eV; panel (b): no fields and $\Delta_c=0.3$ eV; panel (c): piezoelectric fields and $\Delta_c=0$ eV; panel (d): piezoelectric fields and $\Delta_c=0.3$ eV. The transition energies are also reported.

A. Spontaneous polarization

Besides piezoelectric polarization, the spontaneous polarization of wurtzite nanorod has been deeply investigated because a large dipole moment can be expected in these systems.[16–18,21] In Fig. 6 we report the computed spontaneous polarization potential inside a CdS nanorod. This potential has been computed by solving the three-dimensional Poisson equation (as described above) considering the sur-

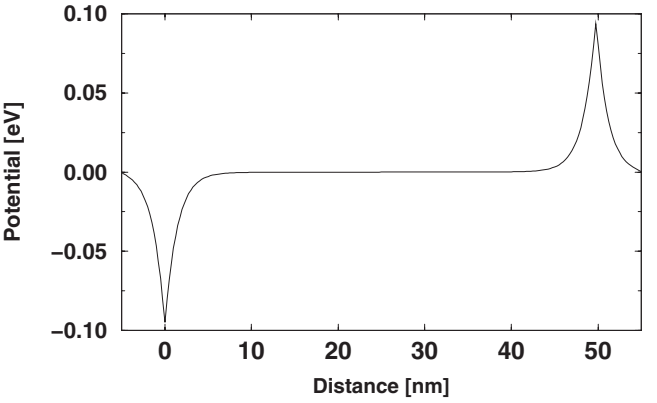

FIG. 6. Electrostatic potential from spontaneous polarization charges of a CdS rod along the rod long axis.

face polarization charges[17] at the ends of the nanorod. We note that in contrast to polarized spheres or quantum wells,[26] we do not obtain a linear potential profile (we recall that the electric field of an uniformly polarized sphere is uniform, and in polarized quantum-well "planes" of uniformly distributed surface charges are present).

In the case of a long nanorod, such as that considered here, the internal electrostatic potential can be approximated by two "point" charges at the ends of the rods, i.e., $V(x)=q/x-q/(x+L)$, where $0<x<L$, L being the length of the rod and $q=P_sA$, with A being the area of the basal facet of the rod. In this case the point charges at the ends of the rod create an electrostatic potential different from zero only close to the ends of the nanorod, whereas inside the nanorod (i.e., at the CdSe core position) the electrostatic potential is almost zero. Therefore, for a long nanorod the electronic wave functions are almost unaffected by the presence of the spontaneous polarization and no significant intrinsic Stark effect can be found. We thus can correctly consider only the internal piezoelectric field as origin of the internal electric field.

V. DISCUSSION

In the flat-band case [see Fig. 5(a) and 5(b)], i.e., without any internal electric field, blueshift of the photoluminescence at high excitation density could only originate from multiexcitonic effects.[53–55] In fact, as recently reported on colloidal type-II systems[59,60] and often observed on epitaxial self-assembled nanostructures[61–63] a blueshifted emission with increasing the excitation power can be related to biexcition emission.

In the case of $\Delta_c=0$ eV (panel a) the electron-hole overlap is very small due to the delocalization of the electron in the shell. In this case very large biexcitonic effects are expected, and in fact from Eq. (3) we obtain $B_{XX}=-143$ meV. Despite the shortcomings of the effective-mass approximation and of the first-order perturbation theory, these results clearly indicate that a quite large biexciton binding energy should be present, which lead to a well resolved additional peak in the PL spectrum at high power.[59,60] But this peak is not observed, since all the spectra can be well fitted by Lorentzian and Gaussian curves for single and ensemble of NCs, respectively. This probably means that a zero conduction-band offset is not appropriate for these systems.

In the case of $\Delta_c=0.3$ eV, the electron and hole states are well localized in the core, thus positive biexciton binding energies are expected,[53–55,64,65] in contrast to the observed blueshifted emission. Note that in this case the biexciton binding energy cannot be computed using Eq. (3) (we obtain $B_{XX}=-5$ meV) due to the neglect of correlation effects.[53,54] Moreover, the biexciton binding energy depends also on the number of confined states. More (less) confined states increase (decrease) the correlation contribution leading to positive (negative) binding energies. Rodt and co-workers[61,62] found a transition to an (very small) antibinding energy when only one hole state lies in the dot. However, in our CdSe core several quantized hole states are found in the core due to the large valence-band offset,[9,13] again meaning that positive biexciton binding energies are expected.

Thus previous discussion indicates that the present experimental data cannot easily be justified with a biexcitonic emission and more accurate investigations are required. Here we propose an alternative explanation for the experimental blueshift.

The electronic structure of these NCs can be modified by the presence of an internal field, which could arise from the spontaneous and/or piezoelectric polarization related to the wurtzite crystalline structure.[21] In Sec. IV A we showed that the electrostatic potential due to the spontaneous polarization, if not screened by the presence of organic surfactants, will have negligible effects on the electronic structure.

Therefore, a possible source of the internal field arises from the piezoelectric polarization charges present at the CdSe/CdS interfaces.

With piezoelectric field, there are two possible effects that lead to a blueshifted emission.

(1) *Piezoelectric effects on biexcitons.* As in epitaxial InAs/GaAs QDs (Refs. 61–63) the piezoelectric potential might shift the biexciton binding energy from positive to negative.

However, we point out that our CdSe core is very small (4 nm) and has a spherical shape in contrast to typical InAs QD which has larger dimension and a (truncated) pyramidal shape. In the case of large InAs QD the overlap between the electron and hole can be very small so that Coulomb repulsion overcomes correlation effects leading to negative biexciton binding energies.[63] In our small CdSe core this is not expected because the electron-hole overlap is still very large due to the small size and the large valence-band offset. Calculation of biexciton binding energies using Eq. (3) is not accurate enough due to the neglect of large correlation effect due to the presence of several quantized hole states (see above), which should lead to a positive biexciton binding energy. Moreover, as stated above, no biexction peak is found in the PL spectra.

(2) *Free-carrier screening of the polarization charges.* As it happens in GaN quantum dots[24] and quantum wells[26,27] the photoexcited electron-hole pairs can screen the piezoelectric potential. In an ideal completely screened situation, the measured blueshift is related to the difference between the transition energy with and without the piezoelectric field, which in the case of $\Delta_c=0.3$ eV [22 meV, see Fig. 5(d)] is in perfect agreement with the measured value of E_{sat} [Fig. 3(b)]. In the case of $\Delta_c=0.3$ eV an almost complete screening of the polarization field can be indeed achieved (and with few electron-hole pairs) due to the large conduction and valence-band offset. However, we point out that the exact value of the piezoelectric shift cannot be computed because it strongly depends on many parameters (such as the strain at the interfacial region and the shell thickness) which might depend on the growth process or are experimentally known only with large uncertainness. In fact, the shift was found to be different from rod to rod, ranging from 14 to 32 meV. A more refined self-consistent calculation[24,26] for different number of electron-hole pairs is in progress and it will be published elsewhere.

We can thus propose that the measured blueshift is related to a photoinduced screening of an internal piezoelectric field. In particular, the transient redshift of the PL emission (see

Fig. 3), similar to those reported on GaN-based structures,[28,30] is related to a photoinduced dynamical descreening of the polarization field. In our case, the time dependence of the emission energy is logarithmic[22] [see Fig. 3(b)] as a consequence of the temporal decay of the carrier population and, therefore, of the photoinduced screening due to the spatial separation of the electrons and holes. The shifts observed as a function of power [inset of Fig. 3(b)] give a measure of the strength of the screening that is generated at different excitation densities, and a saturationlike behavior is expected for a maximum screening. Other possible sources of the internal field could be trapped charges, whose determination and characterization are quite difficult.

The previous discussion also holds for spheres, which have a total diameter of 20 nm. The measured blueshift is smaller (18 meV) and can be assigned to the increased volume with respect to the rods, which reduces the electron quantization energies or dielectric effects in the electronic energy levels.[51,52]

VI. CONCLUSIONS

Single nanoparticle and TRPL spectroscopies show an optical nonlinearity consisting in a systematic blueshift of single dot/rod spectra with increasing excitation density and a dynamical, power-dependent redshift of the ensemble spectra undergoing a saturation behavior. The reversibility of the experiments and the computation of the biexciton binding energy rule out photodegradation and biexcitonic emission as cause of the observed nonlinearity and assign its origin to the screening of an internal electric field. This originates from the piezoelectric polarization due to the strain induced by the lattice mismatch at the core/shell interface. The PL time decays recorded at low excitation density show an exponential decay with typical lifetimes of 11–12 ns, ascribable to the exciton radiative recombination. With increasing excitation power, an additional, faster component appears. The analyses of both the lifetime and the relative contribution over the power suggest it is due to multicarrier recombination via Auger mechanisms.

ACKNOWLEDGMENTS

We would like to thank Paolo Cazzato for valuable technical assistance, Isabella Franchini for help in the chemical synthesis, and Concetta Nobile and Stefania D'Agostino for helpful discussion. This work was supported by the European Project SA-NANO (Contract No. 013698) and by the Italian Ministry of Research (Contract No. RBIN048TSE).

*Corresponding author; giovanni.morello@unile.it

[1] L. Qu and X. Peng, J. Am. Chem. Soc. **124**, 2049 (2002).
[2] P. D. Cozzoli, T. Pellegrino, and L. Manna, Chem. Soc. Rev. **35**, 1195 (2006).
[3] S. Coe, W. K. Woo, M. G. Bawendi, and V. Bulovic, Nature (London) **420**, 800 (2002).
[4] N. C. Greenham, X. Peng, and A. P. Alivisatos, Phys. Rev. B **54**, 17628 (1996).
[5] V. I. Klimov, A. A. Mikhailovsky, S. Xu, A. Malko, J. A. Hollingworth, C. A. Leatherdale, H.-J. Eisler, and M. G. Bawendi, Science **290**, 314 (2000).
[6] D. Tarí, M. De Giorgi, F. Della Sala, L. Carbone, R. Krahne, L. Manna, R. Cingolani, S. Kudera, and W. J. Parak, Appl. Phys. Lett. **87**, 224101 (2005).
[7] D. Tarí, M. De Giorgi, P. P. Pompa, L. Carbone, L. Manna, S. Kudera, and R. Cingolani, Appl. Phys. Lett. **89**, 094104 (2006).
[8] D. V. Talapin, J. H. Nelson, E. V. Shevchenko, S. Aloni, B. Sadtler, and A. P. Alivisatos, Nano Lett. **7**, 2951 (2007).
[9] L. Carbone, C. Nobile, M. De Giorgi, F. Della Sala, G. Morello, P. Pompa, M. Hytch, E. Snoeck, A. Fiore, I. R. Franchini, M. Nadasan, A. F. Silvestre, L. Chiodo, S. Kudera, R. Cingolani, R. Krahne, and L. Manna, Nano Lett. **7**, 2942 (2007).
[10] D. V. Talapin, R. Koeppe, S. Götzinger, A. Kornowski, J. M. Lupton, A. L. Rogach, O. Benson, J. Feldmann, and H. Weller, Nano Lett. **3**, 1677 (2003).
[11] S. Pokrant and K. B. Whaley, Eur. Phys. J. D **6**, 255 (1999).
[12] J. Müller, J. M. Lupton, P. G. Lagoudakis, F. Schindler, R. Koeppe, A. L. Rogach, J. Feldmann, D. V. Talapin, and H. Weller, Nano Lett. **5**, 2044 (2005).
[13] D. Steiner, D. Dorfs, U. Banin, F. Della Sala, L. Manna, and O. Millo, Nano Lett. **8**, 2954 (2008).
[14] J. Müller, J. M. Lupton, A. L. Rogach, J. Feldmann, D. V. Talapin, and H. Weller, Phys. Rev. B **72**, 205339 (2005).
[15] R. M. Kraus, P. G. Lagoudakis, A. L. Rogach, D. V. Talapin, H. Weller, J. M. Lupton, and J. Feldmann, Phys. Rev. Lett. **98**, 017401 (2007).
[16] L. S. Li and A. P. Alivisatos, Phys. Rev. Lett. **90**, 097402 (2003).
[17] T. Nann and J. Schneider, Chem. Phys. Lett. **384**, 150 (2004).
[18] M. Shim and P. Guyot-Sionnest, J. Chem. Phys. **111**, 6955 (1999).
[19] S. A. Blanton, R. L. Leheny, M. A. Hines, and P. Guyot-Sionnest, Phys. Rev. Lett. **79**, 865 (1997).
[20] R. Krishnan, M. A. Hahn, Z. Yu, J. Silcox, P. M. Fauchet, and T. D. Krauss, Phys. Rev. Lett. **92**, 216803 (2004).
[21] N. Q. Huong and J. L. Birman, J. Chem. Phys. **108**, 1769 (1998).
[22] W. Langbein, M. Hetterich, and C. Klingshirn, Phys. Rev. B **51**, 9922 (1995).
[23] M. P. Halsall, J. E. Nicholls, J. J. Davies, B. Cockayne, and P. J. Wright, J. Appl. Phys. **71**, 907 (1992).
[24] V. Ranjan, G. Allan, C. Priester, and C. Delerue, Phys. Rev. B **68**, 115305 (2003).
[25] G. Salviati, F. Rossi, N. Armani, V. Grillo, O. Martinez, A. Vinattieri, B. Damilano, A. Matsuse, and N. Grandjean, J. Phys.: Condens. Matter **16**, S115 (2004).
[26] F. Della Sala, A. Di Carlo, P. Lugli, F. Bernardini, V. Fiorentini, R. Scholz, and J.-M. Jancu, Appl. Phys. Lett. **74**, 2002 (1999).
[27] R. Cingolani, A. Botchkarev, H. Tang, H. Morkoc, G. Traetta, G. Coli, M. Lomascolo, A. Di Carlo, F. Della Sala, and P. Lugli, Phys. Rev. B **61**, 2711 (2000).

[28] A. Reale, G. Massari, A. Di Carlo, P. Lugli, A. Vinattieri, D. Alderighi, M. Colocci, F. Sermond, N. Grandjean, and J. Massies, J. Appl. Phys. **93**, 400 (2003).
[29] S. Dhar, U. Jahn, O. Brandt, P. Waltereit, and K. H. Ploog, Phys. Status Solidi A **192**, 85 (2002).
[30] P. Lefebvre, S. Kalliakos, T. Bretagnon, P. Valvin, T. Taliercio, B. Gil, N. Grandjean, and J. Massies, Phys. Rev. B **69**, 035307 (2004).
[31] M. Gurioli, S. Sanguinetti, and M. Henini, Appl. Phys. Lett. **78**, 931 (2001).
[32] C. Morhain, T. Bretagnon, P. Lefebvre, X. Tang, P. Valvin, T. Guillet, B. Gil, T. Taliercio, M. Teisseire-Doninelli, B. Vinter, and C. Deparis, Phys. Rev. B **72**, 241305(R) (2005).
[33] D. Ricard, M. Ghanassi, and M. C. Schanneklein, Opt. Commun. **108**, 311 (1994).
[34] D. Dutton, Phys. Rev. **112**, 785 (1958).
[35] Landolt-Börnstein, *Numerical Data and Functional Relationship in Science and Technology*, New Series, Group III, edited by K. H. Hellwege, Vol. 17, Pt. B (Springer, New York, 1982).
[36] S. A. Empedocles and M. G. Bawendi, J. Phys. Chem. B **103**, 1826 (1999).
[37] G. Schlegel, J. Bohnenberger, I. Potapova, and A. Mews, Phys. Rev. Lett. **88**, 137401 (2002).
[38] S. A. Empedocles, R. Neuhauser, K. Shimizu, and M. G. Bawendi, Adv. Mater. (Weinheim, Ger.) **11**, 1243 (1999).
[39] X. Wang, L. Qu, J. Zhang, X. Peng, and M. Xiao, Nano Lett. **3**, 1103 (2003).
[40] V. I. Klimov, A. A. Mikhailovsky, D. W. McBranch, C. A. Leatherdale, and M. G. Bawendi, Science **287**, 1011 (2000).
[41] I. Robel, B. A. Bunker, P. V. Kamat, and M. Kuno, Nano Lett. **6**, 1344 (2006).
[42] S. A. Crooker, T. Barrick, J. A. Hollingsworth, and V. I. Klimov, Appl. Phys. Lett. **82**, 2793 (2003).
[43] Al. L. Efros, M. Rosen, M. Kuno, M. Nirmal, D. J. Norris, and M. Bawendi, Phys. Rev. B **54**, 4843 (1996).
[44] M. Califano, A. Franceschetti, and A. Zunger, Nano Lett. **5**, 2360 (2005).
[45] In a typical synthesis of CdSe/CdS QDs via seeded growth, 0.055 g of CdO (99.5%; Sigma Aldrich) are mixed in a 50 ml flask together with 3 g of trioctylphosphine oxide (TOPO 99%; Strem Chemicals), 0.290 g of octadecylphosphonic acid (ODPA, 99%; PCI), and 0.085 g of hexylphosphonic acid (HPA 99%; PCI). After pumping the flask to vacuum for about 1 h at 150 °C, the resulting solution is heated to 380 °C under nitrogen. At this step 1.5 g of trioctylphosphine (TOP, 97%; Strem Chemicals) is injected, after which the temperature is allowed to recover to the value required for the injection of the solution of sulfur precursor+nanocrystals. Such solution is prepared by dissolving 0.120 g of sulfur (S 99%; Strem Chemicals) in 1.5 g of TOP and adding to this 425 μl of a 200 μM solution of readily prepared CdSe dots dissolved in TOP (the lowest absorbance energy peak of CdSe dots was at 589 nm). The resulting solution is quickly injected into the flask. After injection, the temperature drops few tens of degrees (25–30 °C) and it recovers within 2 min to the preinjection temperature. The nanocrystals are allowed to grow for about 8 min after the injection, after which the heating mantle is removed.
[46] P. Harrison, *Quantum Wells, Wires and Dots: Theoretical and Computational Physics of Semiconductor Nanostructures* (Wiley, New York, 2005).
[47] T. S. Li and K. J. Kuhn, J. Comput. Phys. **110**, 292 (1994).
[48] G. Pellegrini, G. Mattei, and P. Mazzoldi, J. Appl. Phys. **97**, 073706 (2005).
[49] A. Schliwa, M. Winkelnkemper, and D. Bimberg, Phys. Rev. B **76**, 205324 (2007).
[50] Y. W. Cao and U. Banin, J. Am. Chem. Soc. **122**, 9692 (2000).
[51] V. A. Fonoberov, E. P. Pokatilov, and A. A. Balandin, Phys. Rev. B **66**, 085310 (2002).
[52] A. Franceschetti, A. Williamson, and A. Zunger, J. Phys. Chem. B **104**, 3398 (2000).
[53] A. J. Williamson, A. Francheschetti, and A. Zunger, Europhys. Lett. **53**, 59 (2001).
[54] J. Shumway, A. Franceschetti, and A. Zunger, Phys. Rev. B **63**, 155316 (2001).
[55] P. Hawrylak, Phys. Rev. B **60**, 5597 (1999).
[56] A. Piryatinski, S. A. Ivanov, S. Tretiak, and V. I. Klimov, Nano Lett. **7**, 108 (2007).
[57] X. G. Peng, M. C. Schlamp, A. V. Kadavanich, and A. P. Alivisatos, J. Am. Chem. Soc. **119**, 7019 (1997).
[58] H. Fröhlic, *Theory of Dielectrics* (Oxford University Press, Oxford, 1958).
[59] D. Oron, M. Kazes, and U. Banin, Phys. Rev. B **75**, 035330 (2007).
[60] V. I. Klimov, S. A. Ivanov, J. Nanda, M. Achermann, I. Bezel, J. A. McGuire, and A. Piryatinski, Nature (London) **447**, 441 (2007).
[61] S. Rodt, R. Heitz, A. Schliwa, R. L. Sellin, F. Guffarth, and D. Bimberg, Phys. Rev. B **68**, 035331 (2003).
[62] S. Rodt, A. Schliwa, K. Pötschke, F. Guffarth, and D. Bimberg, Phys. Rev. B **71**, 155325 (2005).
[63] O. Stier, A. Schliwa, R. Heitz, M. Grundmann, and D. Bimberg, Phys. Status Solidi B **224**, 115 (2001).
[64] V. I. Klimov, S. Hunsche, and H. Kurz, Phys. Rev. B **50**, 8110 (1994).
[65] M. Achermann, J. A. Hollingsworth, and V. I. Klimov, Phys. Rev. B **68**, 245302 (2003).